

This is the post-print version of the following article: Sandro Martins de Oliveira, Susana Velasco-Lozano, Alejandro H. Orrego, Javier Rocha-Martín, Sonia Moreno-Pérez, José M. Fraile, Fernando López-Gallego, and Jose Manuel Guisán, [Functionalization of porous cellulose with glyoxyl groups as a carrier for enzyme immobilization and stabilization](#), *Biomacromolecules* 2021, 22, 927–937
DOI: [10.1021/acs.biomac.0c01608](https://doi.org/10.1021/acs.biomac.0c01608)

This article may be used for non-commercial purposes in accordance with ACS Terms and Conditions for Self-Archiving.

Functionalization of porous cellulose with glyoxyl groups as a carrier for enzyme immobilization and stabilization

Sandro Martins de Oliveira^{†,‡}, Susana Velasco-Lozano^{‡,¶}, Alejandro H. Orrego[†], Javier Rocha-Martín[†], Sonia Moreno-Pérez[†], José M. Fraile[§], Fernando López-Gallego^{‡,¶} and Jose Manuel Guisán^{†*}*

[†]Department of Biocatalysis, Institute of Catalysis and Petrochemistry (ICP) CSIC, Campus UAM, Cantoblanco, 28049 Madrid, Spain.

[‡]Heterogeneous Biocatalysis Laboratory, Center for Cooperative Research in Biomaterials (CIC biomaGUNE), Basque Research and Technology Alliance (BRTA), Paseo de Miramón 182, Donostia San Sebastián, Spain

[§] Instituto de Síntesis Química y Catálisis Homogénea (ISQCH), CSIC-University of Zaragoza, Pedro Cerbuna, 12, Zaragoza, Spain

[¶]IKERBASQUE, Basque Foundation for Science, María Díaz de Haro 3, 48013 Bilbao, Spain

[‡]These authors contributed equally

KEYWORDS: immobilization; enzyme stabilization; bio-based carriers; multipoint covalent attachment, biocatalysis

ABSTRACT

The functionalization of the internal surface of macroporous carriers with glyoxyl groups has proven to highly stabilize a large variety of enzymes through multipoint covalent immobilization. In this work, we have translated the surface chemistry developed for the fabrication of glyoxyl-agarose carriers to macroporous cellulose. To that aim, cellulose-based microbeads were functionalized with glyoxyl groups through a stepwise alkoxylation(or alkylation)/oxidation synthetic scheme. This functionalization sequence was analyzed by solid-state NMR, while the scanning electron microscopy of cellulose microbeads reveals that the mild oxidation conditions negligibly affects the morphological properties of the material. Through the optimal functionalization protocol using *rac*-glycidol, we introduce up to 200 μmols of aldehyde groups per gram of wet cellulose, a similar density to the one obtained for the benchmarked agarose-glyoxyl carrier. This novel cellulose-based carrier succeeds to immobilize and stabilize industrially relevant enzymes such as D-amino acid oxidase from *Trigonopsis variabilis* and xylanases from *Trichoderma reesei*. Remarkably, the xylanases immobilized on the optimal cellulose-based materials present a half-life time of 51 hours at 60 °C, and convert up to 90% of the xylan after 4 operation cycles for the synthesis of xylooligosaccharides.

INTRODUCTION

Enzyme immobilization has been employed in industrial biocatalysis for the last 5 decades.^{1,2} In a simplistic way, the vast majority of the immobilization protocols entail the incorporation of biocatalysts (either an isolated enzyme or a whole cell) to solid materials to primarily ease the separation of the products and exert control over the reaction process. So, an immobilized enzyme can be considered as heterogeneous biocatalyst where the catalysis takes place at the solid-liquid interface. The immobilization itself does not guarantee the stabilization of the resulting heterogeneous biocatalysts unless rational protocols are designed for that purpose.³ Enzyme immobilization is not trivial and so, several parameters must be considered to optimally immobilize enzymes on solid carriers.⁴ Among these parameters the nature of the carrier and the immobilization chemistry are the most crucial ones to preserve the activity and enhance the stability upon the immobilization process.⁵

Sugar-based biopolymers such as agarose have proven excellent carriers for enzyme immobilization due to their biodegradability, hydrophilicity and easy functionalization.⁶ Agarose materials can be functionalized with a plethora of chemical groups to immobilize enzyme through different chemistries. Furthermore, these protein carriers can be presented as cross-linked macroporous beads with suitable mechanical stability to use them in different reactor configurations. Noteworthy, agarose porous microbeads are the benchmark material for protein purification, which can be considered as some sort of a reversible immobilization process.⁷ For protein purification, the immobilization must be reversible to allow the protein elution, so the matrix can be re-used for many purification cycles where a high-value product is obtained (purified proteins). On the contrary, for the fabrication of heterogeneous biocatalysts intended for chemical manufacturing, irreversible immobilization protocols are preferred since they avoid reaction media

contamination due to enzyme leaching and normally increase the enzyme stability.⁵ In this context, the carrier must be disposed when the enzyme is inactivated, which is dramatic in economic terms, when the final products have low-medium market value. So, the cost of the carrier has a great impact on the process economics.⁸ Therefore, we need to seek for more economic alternatives as carriers for enzyme immobilization. Cellulose can be an excellent, abundant, and renewable material source to prepare carriers for enzyme immobilization.⁹ Nevertheless, raw cellulose cannot be directly use for that purpose due to its crystallinity, inertness and microporosity.¹⁰ Luckily, material sciences have advanced in crafting cellulosic materials to fabricate macroporous particles with excellent properties for enzyme immobilization.¹¹ Furthermore, the chemical structure of this material has been altered to introduce a handful of reactive groups.¹¹ Nowadays, many companies supply these cellulose-based particles for enzyme immobilization with a cost 300% lower than agarose macroporous beads. Moreover, cellulose presents better mechanical properties than agarose-based materials, which makes the former more suitable to work under continuous operation at high flow-rates with lower back pressures.¹²

Immobilization of enzymes through aldehyde groups promotes an outstanding stability in the resulting heterogeneous biocatalysts.¹³ Using these carriers, the target enzyme is immobilized through the nucleophilic attack of primary amine groups of the proteins (mainly the ϵ -NH₂ of the lysines) to the aldehydes displayed at the carrier surface under alkaline conditions. As result, reversible imine bonds are formed, being subsequently reduced to irreversible secondary amines using mild-reducing agents like sodium borohydride or boranes. The enzyme stabilization obtained with this immobilization protocol relies on a multivalent attachment between enzymes and carriers. Glyoxyl agarose has proven to enhance the stability of a myriad of enzymes through the aldehyde

chemistry above described, achieving immobilized enzymes 10^5 times more stable than their soluble counterparts.¹⁴

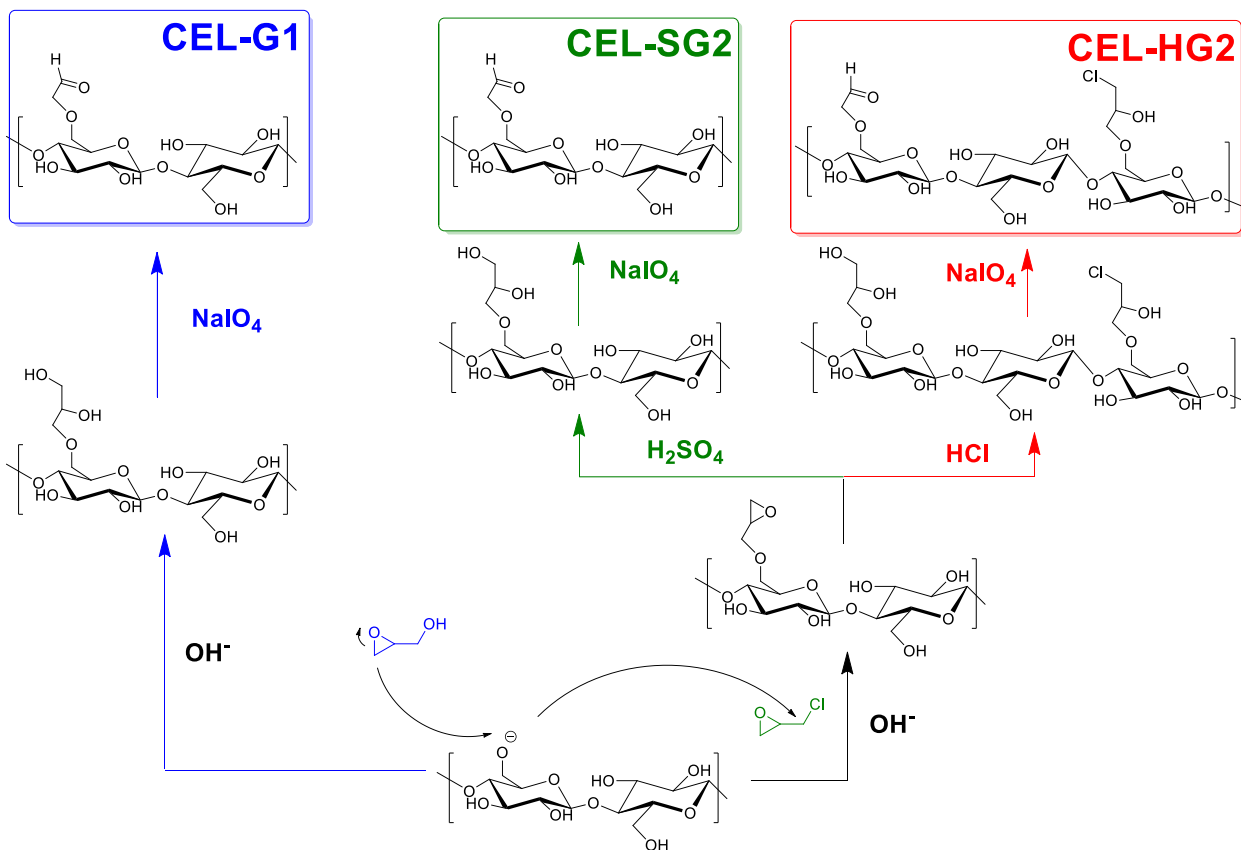
In this work, we intend to transfer the protocols historically developed to prepare glyoxyl agarose, to commercially available cellulose macroporous particles. We have chemically and morphologically characterized the cellulose microbeads activated with aldehyde groups through a step-wise alkylation/oxidation synthetic scheme. Finally, these materials were applied for covalent and irreversible immobilization of two industrially relevant enzymes; the D-amino acid oxidase from *Trigonopsis variabilis* (TvDAO) widely exploited for the synthesis of semi-synthetic β -lactam antibiotics¹⁵ and the xylanases from *Trichoderma reesei* (Xyl) used in the xylan degradation for biomass valorization,¹⁶ as well as for the sustainable and selective synthesis of xylooligosaccharides (XOS).¹⁷

RESULTS AND DISCUSSION

Activation of cellulose-based macroporous beads with aldehyde (glyoxyl) groups

Based on the consolidated surface chemistry developed to functionalize agarose-based materials, we expanded this chemistry to cellulose. To this aim, we functionalized cellulose porous particles (100-250 μm) with aldehyde groups to further promote multipoint-irreversible protein immobilization. The vicinal 2,3 diol of the β -D-glucose monomers forming the cellulose fibers can be directly oxidized to aldehydes under aqueous conditions using sodium periodate as oxidant.¹⁸ Such oxidation step requires drastic conditions to achieve high densities of aldehyde groups, but negatively affects both the morphology and the mechanical properties of the polymeric mesh.^{18, 19} As alternative, the C6 primary hydroxyl groups of the β -D-glucose monomers forming cellulose can be alkylated with vicinal diols to be further oxidized, and so increase the density of

aldehyde groups in the cellulose fibers without deteriorating the cellulose structure. To that end, we followed two strategies using either *rac*-glycidol or epichlorhydrin as reagents to form CEL-G1 or CEL-(H/S)G2, respectively (**Scheme 1**)



Scheme 1. Different activation pathways of glyoxyl-cellulose microbeads. CEL-G1 (blue arrows) pathway involves two steps; 1) the alkylation of the C6 of the glucose with *rac*-glycidol and 2) the mild oxidation of the formed vicinal diols (glyceryl groups). CEL-SG2 and CEL-HG2 pathways involve three steps; 1) the Williamson reaction of the glucose C6 hydroxyl with *rac*-epichlorohydrin, 2) the acid hydrolysis using either HCl (red arrows) or H_2SO_4 (green arrows) of the formed epoxides, and 3) the mild oxidation of the formed vicinal diols (glyceryl groups).

In the first case, the C6 primary alcohols are deprotonated under basic and reducing conditions to form the corresponding alkoxides that carry out the nucleophilic attack to the 2,3-oxirane ring of glycidol (alkoxylation), activating the cellulose fibers with 1,2-vicinal diols (glycerol groups) that are further oxidized with NaIO₄ (CEL-G1). In the second case, cellulose was functionalized with epichlorhydrin (EPI), which also activates the C6 hydroxyl groups of the β -D-glucose monomers. Herein, the Cl atom of EPI acts as leaving group upon the attack of the C6 alkoxide of glucose monomers under basic conditions (Williamson synthesis). As result, the C6 hydroxyl group of the glucose monomers is activated with oxiran-2-ylmethoxy groups. Then, the oxirane (epoxide) groups need to be hydrolyzed under acidic conditions to form the vicinal diols (glyceryl groups) that are ultimately oxidized to aldehydes (glyoxyl groups) using sodium periodate. Depending on the acid utilized for the hydrolysis step, we dubbed the resulting materials as CEL-HG2 and CEL-SG2 when using HCl and H₂SO₄, respectively.

In order to titer the number of aldehydes introduced in the cellulose structure, we colorimetrically quantified the consumption of sodium periodate after the oxidation step. Since the oxidation reaction is stoichiometric, we know that one molecule of diol is oxidized by one molecule of NaIO₄. **Table 1** shows the density of aldehydes introduced through the different functionalization methods. When plain cellulose microbeads were oxidized, the density of aldehyde groups was $70 \mu\text{mol} \times g_{\text{carrier}}^{-1}$ as result of the partial oxidation of the C2-C3 vicinal diols forming the chemical structure of cellulose. On the contrary, the functionalization with either glycidol or EPI before the oxidation step allowed ramping the aldehyde density up to $200 \mu\text{mol} \times g_{\text{carrier}}^{-1}$. We suggest that both intrinsic cellulose C2-C3 diols and the newly introduced glyceryl groups at C6 can be oxidized to yield the final aldehydes groups. Using EPI as reagent, we needed to hydrolyze the epoxide groups with H₂SO₄ (CEL-SG2) for 16 hours to achieve the highest

aldehyde density. Acidic hydrolysis steps for shorter times, and the use of HCl as acid (CEL-HG2) resulted in aldehyde densities 30-50% lower than larger incubation times with sulphuric acid. Under these optimal conditions, the total density and reactivity of the aldehyde groups in cellulose porous microbeads are similar to the ones obtained with the conventional protocol using 10 BCL agarose porous microbeads (AG-G) ($200 \mu\text{mol} \times g_{\text{agarose}}$)

Table 1. Colorimetric titration of the aldehyde density in cellulose porous microbeads.

Entry	Material	Activation/Hydrolysis (time/hours)	Aldehydes ($\mu\text{mol} \times g_{\text{carrier}}^{-1}$) ^c
AG-G	Agarose 10BCL	Glycidol/none	200±1
CEL-G		none/none	70±1
CEL-G1		Glycidol/none	200±1
CEL-SG2 ^a	Cellulose MT200	EPI/H ₂ SO ₄ (16)	199±1
CEL-SG2 ^b		EPI/H ₂ SO ₄ (2)	105±1
CEL-HG2		EPI/HCl (16)	155±2

^aMacroporous cellulose beads functionalized with epichlorhydrin and hydrolyzed with H₂SO₄ for 16 hours. ^bMacroporous cellulose beads functionalized with epichlorhydrin and hydrolyzed with H₂SO₄ for 2 hours. ^cAldehyde groups were quantified through NaIO₄ consumption in the supernatant after the oxidation step.

All these cellulose based carriers were analyzed through solid-state NMR to characterize the different chemical transformations occurred during the activation/oxidation steps (**Figure 1**). As standard sample to assign the peaks corresponding to the epoxy, glyceryl and aldehyde groups, we activated silica following the same protocols (epoxidation/hydrolysis/oxidation) used for the synthesis of both CEL-SG2 and CEL-HG2 (**Figure S1-S5**). The ¹³C CP-MAS-NMR spectrum of the silica particles after the epoxide anchoring step shows that the epoxide carbon atoms in the

glycidoxy group appear at 44.6 and 51.6 ppm, whereas the remaining carbon appears in the zone of 73 ppm (**Figure S1**).²⁰ After both hydrolysis and oxidation steps, the expected signal at 203 ppm, corresponding to the carbonyl group of the aldehyde, is hardly visible, whereas at least two peaks appear at 89.5 and 96.1 ppm (**Figures S4 and S5**). These peaks indicate the existence of the aldehydes in the form of hydrate (-CH(OH)₂), as it happens in solution with nucleobase aldehydes (87-89 ppm)^{21, 22} and prolinal derivatives (91.7 ppm).²³ In the same way, the ketone hydrate of phenylpyruvic acid appeared at 98 ppm in solid state NMR.²⁴ When the cellulose microbeads were treated with EPI, solid NMR spectrum (**Figure 1A, bottom**) reveals two signals at 45.6 and 52.1 ppm, in agreement with the presence of the epoxide, according to the silica standard (**Figure S1**). Unfortunately, the signal at 73 ppm could not be assigned as it overlaps with those signals from C2, C3 and C5 of glucose units.²⁵ Remarkably, the ¹³C CP-MAS-NMR spectrum of glycidoxy-cellulose hydrolyzed with HCl shows a new signal at 47.2 ppm, which does not correspond with any alcohol or ether group, but it is consistent with a -CH₂Cl group, resulting from the epoxide ring opening with HCl (**Figure 1B, top**), analogously to the peaks found in the glycidoxy-silica hydrolyzed with the same protocol (**Figure S2**). Hence, solid-state NMR demonstrates that the hydrochloric acid opens the epoxide groups to the 2,3-dihydroxypropyl (vicinal diol) but also to the 3-chloro-2-hydroxypropyl. The signal assigned to the presence of a chlorine atom is absent in the NMR spectrum of the epoxy-cellulose hydrolyzed with H₂SO₄ (**Figure 1B, bottom**). The transformation of epoxides into alkyl chlorides instead into vicinal diols is detrimental for the final density of aldehyde groups after the oxidation step (**Figure S4**), as supported by the titration experiment shown in **Table 1**.

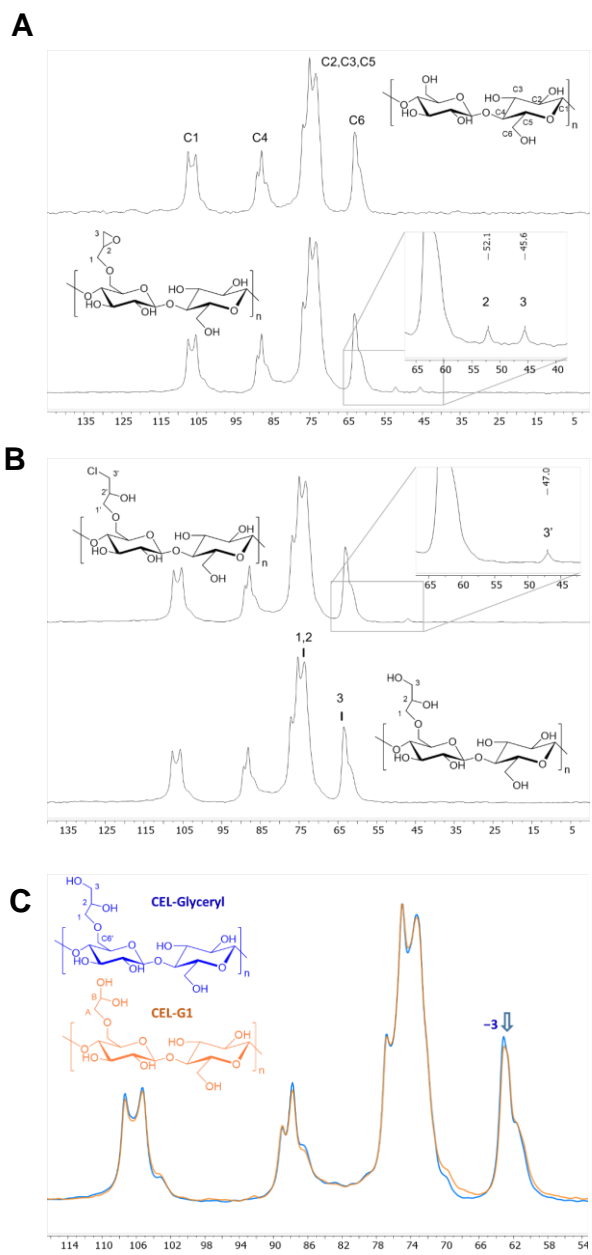


Figure 1. ^{13}C CP-MAS-NMR spectra of different cellulose-based carriers. **(A)** Cellulose microbeads (top) and glycidoxy-cellulose (bottom). **(B)** Glycidoxy-cellulose hydrolyzed with HCl (top) or H₂SO₄ (bottom). **(C)** Overlapped spectra of cellulose after being activated with glycidol (blue), and oxidized with NaIO₄ (glyoxy-cellulose, CEL-G1, orange).

Finally, the oxidation of the hydrolyzed glycidoxy-cellulose samples produces minor but detectable changes in the spectrum (**Figure 1C**). The signal of carbon 3 of glyceryl group (65-59 ppm band) slightly decreases, while the signal corresponding to the aldehyde hydrate (96-89 ppm zone) was not detected, as they overlap with the much more intense signals of C4 atoms of cellulose (91-84 ppm). On the contrary, the spectrum of the analogous agarose derivative after oxidation (**Figure S6**) shows a peak at 89.6 ppm, in agreement with the main peak obtained from 3-glycidoxypropylsilica and assigned to aldehyde hydrates ($-\text{CH}(\text{OH})_2$) groups (**Figure S5**).

SEM analysis of all the samples evidenced that the cellulose matrix suffers negligible morphological changes after activation and oxidations steps (**Figure 2**). In our case, 1 gram of wet cellulose contains 0.12 g of dry cellulose, which means 0.74 mmol of glucose per gram of wet cellulose. Since each molecule of glucose contains one intrinsic vicinal diol plus one extra glyceryl group added during the alkylation process, the maximum amount of vicinal diols that can be potentially oxidized is 1.48 mmol per gram of wet cellulose, yet we add only 0.2 mmol of oxidant per gram. Accounting for the aldehyde densities shown in Table 1, we estimate that the oxidation of non-functionalized cellulose ($70 \mu\text{mol} \times \text{g}_{\text{wet}}^{-1}$) only involves 10% of all glucose monomers, while the oxidation of cellulose functionalized with vicinal diols at C6 ($200 \mu\text{mol} \times \text{g}_{\text{wet}}^{-1}$) modifies up to 27% of the total glucose units. Under these conditions, we avoided the overoxidation of the material that provokes glucose ring-opening, changes in fiber dimensions, and formation of inter- and intrafibrillar hemiacetal as observed when high excess of periodate is used.¹⁸ Both the aldehyde density and the morphology of the functionalized cellulose matrix are similar to the ones established for agarose beads using common protocols. Remarkably, EDX analyses (**Figure S7**) of the cellulose microbeads corroborate the presence of Cl atoms in the cellulose microbeads hydrolyzed with HCl (CEL-HG2), confirming that such acid transforms the epoxides into a

mixture of diols and hydroxy alkyl chlorides. The latter ones were not oxidized, thus reducing the final aldehyde density (**Figure S4**). For this reason, we discarded CEL-HG2 carrier, and selected CEL-G1 and CEL-SG2 hydrolyzed for 16 hours as the best carrier for further immobilization experiments.

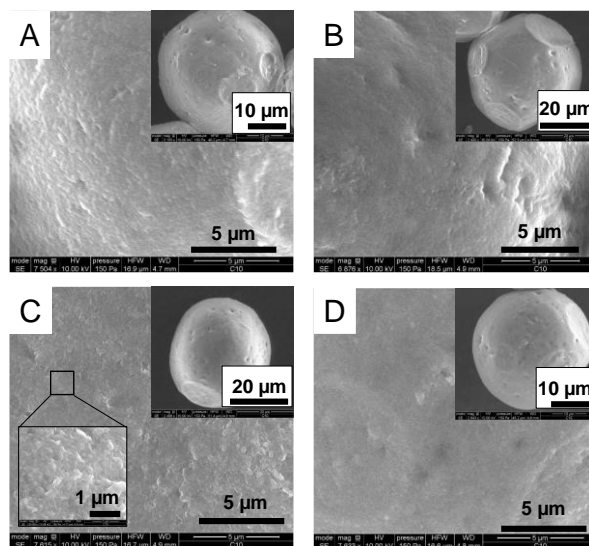


Figure 2. SEM micrograph of different cellulose-based carriers at 7000X magnification. A) Plain cellulose (CEL) microbeads. B) Glyoxyl-cellulose (CEL-G1) microbeads. C) Epoxy-cellulose microbeads hydrolyzed with H_2SO_4 and oxidized with NaIO_4 (CEL-SG2). D) Epoxy-cellulose microbeads hydrolyzed with HCl and oxidized with NaIO_4 (CEL-HG2). In the insets, the micrographs of the same samples at 2500-3000 X magnification are shown. In addition, panel C also shows a micrograph with 30000X magnification to visualize the porous microstructure of CEL-SG2

Immobilization of enzymes on cellulose porous microbeads activated with aldehydes (glyoxyl groups)

As model enzyme, we immobilized the D-aminoacid oxidase from *Trigonopsis variabilis* (TvDAO) on both CEL-G1 and CEL-SG2 under alkaline conditions. **Table 2** shows that cellulose-based matrixes immobilized 20-25% less enzyme than the benchmark agarose-based matrix for multipoint covalent immobilization. On the contrary, the recovered activities of TvDAO immobilized on both CEL-G1 and CEL-SG2 were similar to one recovered upon its immobilization on AG-G; 60% of the activity measured for the free enzyme under the same conditions (**Table 2**). These immobilization parameters were also similar to those ones found for the same enzyme immobilized on agarose-based carriers activated with sodium cyanogen bromides (**Table 2**), that are well known to immobilize proteins through their N-terminus, establishing an univalent irreversible interaction between the proteins and the carriers.¹⁴

Table 2. Parameters for the immobilization of TvDAO on different carriers.

Carrier	Load (mg _{TvDAO} x g _{carrier} ⁻¹)	Immobilization yield (%)	Relative Recovered Activity (%)
AG-G ^a	1	99±3	58±3
CEL-G1 ^a	0.8	80±1	52±3
CEL-SG2 ^a	0.74	74±2	49±2
AG-CB ^b	0.87	87±4	62±2

^aEnzymes were contacted with the carrier for 3 hours in 0.1 M sodium bicarbonate pH 10 at 25°C. Upon the immobilization, the samples were incubated with 1 mg x mL⁻¹ NaBH₄ for 0.5 hours at 25 °C. ^bEnzymes were contacted with the carrier for 2 hours in 0.1 M sodium phosphate pH 7 at 25 °C. Upon the immobilization, the samples were incubated with 1 M ethanolamine at pH 8 for 2 hours at 25 °C.

Since the functional properties of TvDAO immobilized on both agarose and cellulose matrix were similar, we suggest that AG-G, AG-CB, CEL-G1 and CEL-2SG capture similar protein conformation upon the immobilization process. This suggestion is supported by the similar Trp fluorescence spectra recorded for the immobilized enzymes (**Figure S8**). Surprisingly, all these supported enzymes exhibit quite different behaviors under temperature inactivation conditions. While TvDAO immobilized on AG-G presented a half-life time of 4.57 hours (**Table S1**), the same enzyme immobilized on CEL-SG2 and CEL-G1 was 8-10 times less stable, but 20% more stable than the enzyme immobilized on AG-CB (**Figure 3A**). The stabilization promoted by AG-G is supported by a 4 °C higher T_m according to the thermal denaturation studies (**Figure 3B and Figure S9**).

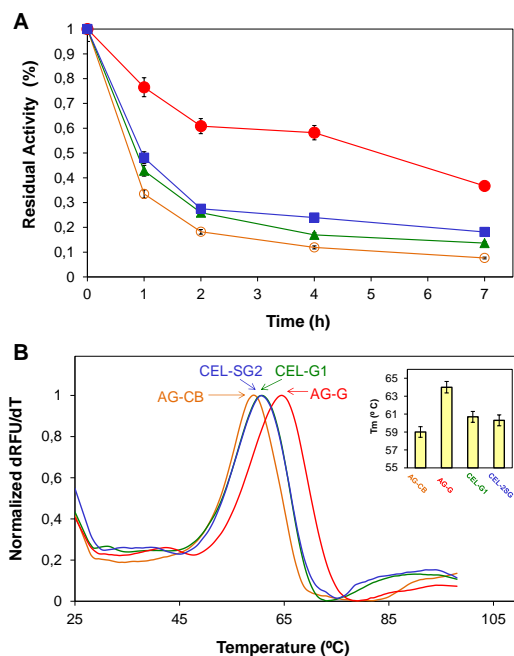


Figure 3. Thermal inactivation of TvDAO immobilized on different carriers. **(A)** Kinetic thermal inactivation at 50 °C and pH 7 **(B)** thermodynamic denaturation of different heterogeneous biocatalysts of TvDAO. The inset shows the values of the melting temperature for the different

samples. TvDAO immobilized on AG-CB (orange), on AG-G (red), on CEL-SG2 (blue), and on CEL-G1 (green).

To test the universality of this cellulose matrix activated with glyoxyl groups, we immobilized a cocktail of xylanases from *Trichoderma reesei* (Xyl) on CEL-G1 and CEL-SG2 and compared them with the immobilized preparation using AG-CB (univalent immobilization) and AG-G (**Table 3**). Unlike TvDAO, only 14% of Xyl was immobilized on CEL-G1 after 4 hours, whereas the AG-G was able to immobilize 80% of the offered protein under the same immobilization time and conditions. To maximize the immobilization of Xyl on CEL-G1, we studied the effect of the incubation time on the immobilization yield. After 24 hours, the immobilization yield was roughly 80% and it did not significantly increase doubling the immobilization time.

Table 3. Parameters for the immobilization of Xyl on different carriers.

Carrier	Load (mg _{Xyl} x g _{carrier} ⁻¹)	Immobilization time (hours)	Immobilization yield (%)	Relative Recovered Activity (%)
AG-G ^a	8.1	4	90±3	89±3
	1.3	4	14±5	99±10
CEL-G1 ^a	7.6	24	84±2	49±3
	8.0	48	89±5	47±5
CEL-SG2 ^a	7.0	24	78±7	14±1
AG-CB ^b	3.0	0.33	31±3	100±10

^aEnzymes were contacted with the carrier in 0.1 M sodium bicarbonate pH 10 at 25 °C. Upon the immobilization, the samples were incubated with 1 mg/mL NaBH₄ for 0.5 hours at 25 °C.

^bEnzymes were contacted with the carrier in 0.1 M sodium phosphate pH 7 at 25 °C. Upon the immobilization, the samples were incubated with 1M ethanolamine at pH 8 for 2 hours at 25 °C. In all cases, 9 mg of protein were offered to 1 gram of each carrier.

Interestingly, the immobilization of Xyl on CEL-SG2 for 24 hours reached similar yield but the immobilized enzyme recovered 3.5-fold less activity than those immobilized on CEL-G1. Since we did not observe the inactivation of TvDAO when it was immobilized on CEL-SG2 (**Table 2**), an explanation for the negative effect found with Xyl, would be too speculative and premature at this time. Despite not fully understanding why CEL-G1 retains higher Xyl activity, we selected this carrier for further studies. In terms of immobilization parameters, CEL-G1 is able to immobilize as much Xyl as AG-G but demanding longer immobilization times and yielding immobilized enzymes roughly 2 times less active. Interestingly, the recovered activity of Xyl on CEL-G1 was also lower than the activity exhibited by this enzyme upon the immobilization on AG-CB. As Xyl recovered similar activity upon its immobilization on both AG-G and AG-CB, we suggest that increasing the number of covalent bonds between the Xyl and the carrier negligibly affects the enzyme activity. Hence, the inactivation undergone by Xyl during the immobilization on CEL-G1 might rely on the longer incubation time under alkaline conditions demanded by this carrier to achieve high immobilization yields.²⁶ In fact, free Xyl lost all its activity after 48 hours of incubation at pH 10 and 25° C (**Figure S10**) as reported for other xylanases inactivated under alkaline conditions^{27, 28}.

To unveil whether the glyoxyl chemistry was promoting different conformational changes on Xyl immobilized on AG-G and CEL-G1, we recorded the Trp-fluorescence spectra of the immobilized biocatalysts (**Figure S11**). The normalized spectra showed a significant 5 nm red-shifted maximum emission peak (λ_{max}) in Xyl immobilized on AG-G regarding the same enzyme immobilized on CEL-G1. Likewise, the maximum fluorescence intensity at the λ_{max} dramatically decayed when the enzyme was immobilized on AG-G. All these spectral changes suggest notable

structural distortions on Xyl when immobilized on AG-G compared to CEL-G1. Surprisingly, those conformational changes conducted to more active enzymes.

To assess the conformational stability of Xyl immobilized on both AG-G and CEL-G1, we performed thermodynamic and kinetic stability tests (**Figure 4**). The thermal denaturation studies showed that T_m of Xyl immobilized on CEL-G1 was 10 °C lower than Xyl immobilized on AG-G. Remarkably, **Figure 4A** shows two populations of immobilized Xyl on AG-G according to the two peaks identified through the first derivative plot (dF/dT). Higher T_m points out that AG-G promotes the stabilization of Xyl to a higher extent than CEL-G1. The high stability of Xyl immobilized on agarose matrix is manifested in the kinetic inactivation courses (**Figure 4B and Table S2**), where the enzyme immobilized on AG-G presented a half-life time 70 times higher than immobilized on CEL-G1 under the same immobilization time (4 hours). To achieve a Xyl stability similar to the agarose carriers, the enzymes needed to be incubated with CEL-G1 for up to 48 hours. As result, the Xyl immobilized on CEL-G1 for 48 h preserved 60% of its initial activity after 24 hours, while the activity of the free enzyme decayed 86% under the same inactivation conditions. Thus, CEL-G1 requires longer times to achieve high immobilization yields but also to establish enough enzyme-carrier attachments to stabilize the Xyl conformation against denaturing agents such as temperature. Looking deeper into the inactivation time-courses (**Figure 4B**), we observed that Xyl immobilized on AG-G follows a two-stage series inactivation mechanism, where the first inactivation stage defined by the first-order inactivation constant k_1 was 3 order of magnitude faster than the second one defined by the first-order inactivation constant k_2 (**Table S2**).^{29, 30} These differences between the two inactivation constants are also manifested in the thermodynamic thermal inactivation; the two T_m values identified in **Figure 4A** suggest the existence of two enzyme populations with different stability properties. On the contrary, k_1 of the

biocatalyst immobilized on CEL-G1 was only 2 orders of magnitude higher than k_2 . These differences in the inactivation constants seem not to be enough to differentiate two enzyme population in the thermodynamic inactivation experiments.

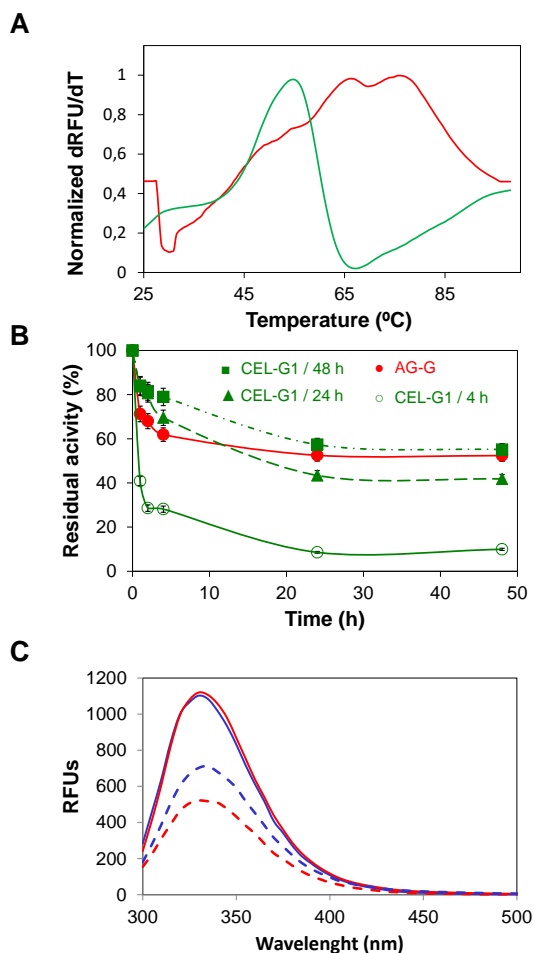


Figure 4. Thermal inactivation of xylanase immobilized on different carriers. **(A)** Thermodynamic denaturation of xylanase immobilized on AG-G (red line) and on CEL-SG2 (green line) for 4 hours. **(B)** Kinetic thermal inactivation at 60 °C and pH 7 of Xyl immobilized on AG-G for 4 hours (red solid line, full circles), on CEL-G for 4 hours (green solid line, empty circle), for 24 h (green dash line, full triangles) and for 48 hours (green dash-dot line, full square). **(C)** The intrinsic fluorescence spectrum was measured before (solid line) and after (dash line) the incubation at 50 °C for 48 hours for the Xyl immobilized on CEL-G1 for 4 hours (red line) and 48 hours (blue line).

Interestingly, the k_1 of Xyl immobilized on AG-G was 12 times higher than its counterpart from Xyl immobilized on CEL-G1 for 48 hours. However, the k_2 of the immobilized biocatalyst on AG-G was slightly higher than the corresponding constant estimated for cellulose-based carrier (**Table S2**). Accordingly, the half-life time of Xyl immobilized on CEL-G1 was 18% higher than the one exhibited by the same enzyme immobilized on AG-G.

Therefore, we have demonstrated that the immobilization time has a significant impact on the final thermal stability of Xyl immobilized on CEL-G1. In the light of these results, we suggest that longer immobilization times establish more bonds between the enzyme and carrier surfaces, which likely avoid drastic structural distortions under high temperature conditions. This fact is supported by the by Trp-fluorescence spectra of Xyl immobilized on CEL-G1 incubated at two different times and recorded before and after 24 hours incubation at 50 °C (**Figure 4C**). The immobilized biocatalyst whose immobilization time is 4 hours suffers a larger reduction of its intrinsic fluorescence than the same biocatalyst immobilized for 24 hours. Both activity and structural data support that moderate temperatures induce dramatic conformational changes in Xyl immobilized on CEL-G1 for shorter times, which negatively affects the performance of the heterogeneous biocatalyst.

Finally, we tested the loading capacity of AG-G and CEL-G1 carriers for Xyl. As result, we found that the cellulose-based materials were able to immobilize similar enzyme loads (40-50 $\text{mg}_{\text{Xyl}} \times \text{g}_{\text{carrier}}^{-1}$) as agarose ones. However, the Xyl immobilized on CEL-G1 recovered only 50% at loadings higher than 9 $\text{mg}_{\text{Xyl}} \times \text{g}_{\text{carrier}}^{-1}$. On the contrary, AG-G better tolerated the high loadings, since we only observed significant reductions of its recovered activity at 5 times higher enzyme loads than the ones found for CEL-G1 (Figure S12).

Operational functional and structural stability of Xyl immobilized on cellulose-based carriers

Despite the low thermostability of TvDAO immobilized on CEL-G1 (Figure 3A), we tested the operational stability of this heterogeneous biocatalyst. Expectedly, we found that 65 % of the initial oxidative activity was lost after the second operational cycle. Such activity decay was linked to the dramatic decrease observed for the maximum protein fluorescence intensity (**Figure 5A**).

On the contrary, Xyl immobilized on CEL-G1 was operationally stable for at least 5 reaction cycles, according to its thermal stability (**Figure 5B**). Previous studies demonstrated that post-immobilization techniques significantly improve the operational performance Xyl immobilized on AG-G.^{31,32} To demonstrate that post-immobilization protocols developed for agarose-based carrier are readily translated to cellulose based carriers, we coated the Xyl immobilized on CEL-G1 for 48 hours with three sequential layers of polymers; polyethylenimine, dextran-aldehyde and aminated PEG. The resulting heterogeneous biocatalyst was exploited for the synthesis of xylooligosaccharides (XOS). As result, the cellulose-based heterogeneous biocatalyst quantitatively converted a solution of xylane in 2 hours with a 91% yield of xylobiose, whereas the same enzyme immobilized on AG-G, and coated with the same polymer layers, needed 3 hours to reach similar yields (Figure S13). Despite recovering lower activity upon the immobilization, the Xyl immobilized on CEL-G1 outperforms the one immobilized on AG-G during the batch-hydrolysis of Xylan.

Finally, we studied the structural stability of Xyl immobilized on CEL-G1 and further coated, during its operational use. To that end, we recorded the Trp-fluorescence spectra before starting the xylan hydrolysis process and after each operational cycle. We observed that the immobilization

and post-immobilization protocols conducted to an immobilized Xyl that only lost 5% of its initial activity after 5 operational cycles. When plotting the fluorescence intensity at the λ_{max} of the two immobilized biocatalysts *versus* the conversion after each operational cycle, we clearly identify an expected correlation between structure and function. As shown in **Figure 5B**, the fluorescence intensity decreases as the Xyl starts to reduce its initial activity after each 2-hour cycle. Although we observed some structural distortion after 5 operational cycles, the enzyme activity was only reduced 4% compared to the activity exhibited in the first cycle. These data support that the immobilization of Xyl on CEL-G1 coated with polymers efficiently preserves the enzyme activity despite some structural distortions occurred during the biocatalyst operational use. Therefore, we demonstrate that the cellulose-based carrier strengthens the enzyme structure, which explains the high operational stability of the heterogeneous biocatalysts herein developed. Hence, the use of a biomass derived carrier allows the stabilization of Xyl to carry out the biotransformation of biomass derived xylan into xylooligosaccharides; highly added-value molecules in food chemistry.

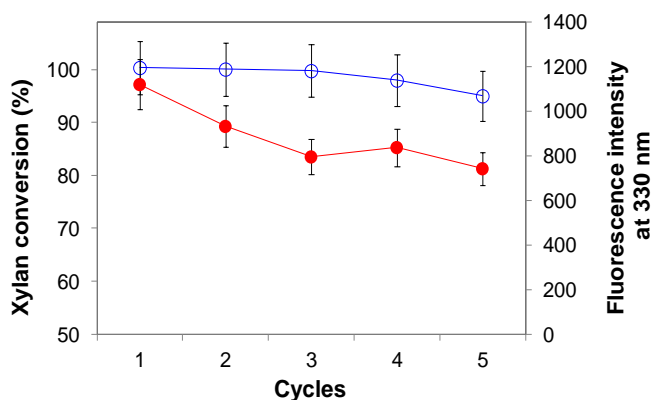


Figure 5. Protein denaturation during the operational use of Xyl immobilized on CEL-G1. Xylan conversion (blue empty circles). Fluorescence emission intensity at 330 nm (red full circles).

CONCLUSION

Functionalization protocols historically developed for agarose have been successfully transferred to activate cellulose macroporous beads with aldehyde groups. We herein optimize the alkylation process to enrich cellulose with vicinal 1,2-diols that ultimately oxidize to generate aldehydes (glyoxyl groups). The mild activation of macroporous cellulose with aldehydes and epoxide groups without deteriorating its morphology and physico-chemical properties means a core functionalization to introduce a variety of reactive groups (amine, thiols, hydrophobic molecules...) into the structure of cellulosic materials. These methodologies pave the path to use cellulose-based materials as carriers for enzyme immobilization and their further use in applied biocatalysis. We demonstrated that the functionalization with *rac*-glycidol yields a similar aldehyde density as with epichlorohydrin, but the resulting carrier (CEL-G1) immobilizes enzyme more effectively. In general, cellulose carriers activated with glyoxyl groups require longer immobilization times than agarose ones to achieve high immobilization yields and stabilize enzymes both thermally and operationally.

EXPERIMENTAL SECTION

Materials

D-aminoacid oxidase from *Trigonopsis variabilis* (TvDAAO) was kindly donated by Recordati, and the Bioxilanase L Plus (Xyl) was provided as a liquid preparation by Biocon (Spain). 10% cross-linked agarose beads (10 BCL) (average particle size: 50-150 μm ; average pore size: 100 nm) was purchased from Agarose Bead Technologies (Madrid, Spain) and Cellulose MT200

(average particle size: 100-250 μm ; average pore size: 32 nm) was purchased from IONTOSORB (Usti and Labem, Czech Republic). Sodium borohydride, sodium periodate, sodium hydroxide, 3,5-dinitrosalicylic acid (DNS), sodium acetate, sodium chloride, sodium phosphate, glycidol, glycerol, D-alanine, horse radish peroxidase (HRP), *o*-phenyldiamine, SYPRO Orange Protein Gel Stain, beechwood xylan and cyanogen bromide-activated sepharose 4B (AG-CB) were purchased from Sigma-Aldrich Chemical Co. (St. Louis, IL, USA). Corncob xylan was purchased from Carbosynth (Berkshire, UK). All other reagents were of analytical grade. D-Alanine, Ammonium Chloride and Catalase from Bovine Liver were purchased from Sigma-Aldrich Co. (St. Louis, IL, USA). NADH was purchased from GERBU Biotechnik GmbH (Heidelberg, Germany). Alanine Dehydrogenase were produced as described elsewhere³³.

Functionalization of cellulose porous microbeads

Alkoxylation with rac-glycidol

100 g of plain cellulose microbeads (CEL) were suspended in 30 mL of distilled water, followed by the addition of 50 mL of NaOH 1.7 M in an ice bath. Afterwards, 1.425 g of sodium borohydride were added. Later, 36 mL of *rac*-glycidol were drop by drop incorporated. The suspension was incubated overnight at room temperature with gentle stirring. Finally, alkoxyated-cellulose beads were fully washed with distilled water, filtered and stored at 4 °C.

Alkoxylation with epichlorohydrin

100 g of CEL were suspended in 160 mL of acetone, followed by the addition of 440 mL of NaOH 1 M containing 2 g of sodium borohydride and maintained in an ice bath. Consecutively, 110 mL of epichlorohydrin were drop by drop incorporated. The suspension was incubated

overnight at room temperature with gentle stirring. Finally, epoxy-cellulose beads were fully washed with distilled water, filtered and stored at 4 °C.

Hydrolysis of epoxide groups to diols

The hydrolysis of the epoxy-cellulose beads was carried out by incubating 1 gram of the resin with 10 volumes of 0.5 M HCl or 0.5 M H₂SO₄ at room temperature for 2-16 hours. After the hydrolysis, cellulose microbeads were fully washed with distilled water and stored at 4 °C.

Oxidation

The oxidations of cellulose activated with diols were conducted by individually suspending 1g of the different activated cellulose microbeads with 10 mL of 20 mM NaIO₄ in distilled water. Suspensions were incubated 1-2 hours at room temperature with gentle stirring up to complete oxidation of the diols. The degree of oxidation was spectrophotometrically determined by measuring the absorbance at 405 nm of the released iodide ions released after its reaction with the remaining NaIO₄ (mixed with 9 volumes of 10% KI in saturated bicarbonate solution (1:1)).³⁴

Functionalization of agarose porous microbeads

AG-G carrier was prepared as previously described.³⁵ The concentration of aldehyde groups was quantified as described for the cellulose-based materials.

NMR studies

CP MAS NMR spectra were recorded in a Bruker Avance III WB400 spectrometer with 4 mm zirconia rotors spun at magic angle in N₂ at 10 kHz. ¹H-¹³C spectra (up to 10000 scans) were measured using a ¹H π/2 pulse length of 2.45 μs, with a contact time of 2 ms, and spinal64 proton decoupling sequence of 4.6 μs pulse length.

SEM/EDX analysis

Scanning Electron Microscope and Energy Dispersive X-ray (SEM-EDX) images were analyzed with a SEM-Quanta FEG-250, ESEM microscope employing a large field detector (LFD). For imaging, 5 μ L of CEL water suspension (1:20) were deposited in the top of carbon conductive tabs. Images were acquired at 10 keV under 150 Pa.

Enzyme Assays

TvDAO colorimetric assay

TvDAO activity in its soluble form was analyzed spectrophotometrically using D-alanine as substrate measuring the increment of absorbance at 445 nm promoted by coupling the oxidative deamination of the substrate with the reaction between the hydrogen peroxide and *o*-phenyldiamine catalyzed by peroxidase.³⁶ The reaction mixture consisted of 1.5 mL of 10 mM D-Alanine solution in 100 mM potassium phosphate at pH 7.5, 0.5 mL of 1.85 mM *o*-phenyldiamine in distilled water and 0.1 mL of a 1 mg/mL peroxidase solution in 50 mM potassium phosphate at pH 7.5. The reagents were preincubated at 25 °C. One DAO unit is defined as the amount of enzyme able to produce one micromole of H₂O₂ per minute under the previously described conditions.

Xylanase colorimetric assay

Xylanase activity was colorimetrically measured by dinitrosalicylic acid (DNS) method, using a suspension of 4% (w/v) beechwood xylan in 50 mM acetate buffer pH 5 according to literature³⁷ with xylose as standard. One unit of enzyme activity was defined as the amount of enzyme required to release 1 μmol of reducing sugars (xylose equivalents) in 1 minute.

Enzyme immobilization on cellulose and agarose carriers functionalized with aldehyde groups

10 mL of 100 mM sodium carbonate pH 10 containing either 1 mg of TvDAO or 9 mg of Xyl were incubated with 1 g of the corresponding carrier at 25 °C for different times (3-48 hours) depending on the enzyme under gently stirring. Upon the immobilization, the samples were incubated with 1 mg \times mL⁻¹ NaBH₄ for 0.5 hours at 25 °C. The same protocol was followed for the immobilization of these enzymes on agarose-based microbeads activated with glyoxyl groups (AG-G)

For the immobilization of enzymes on AG-CB, 1 mg of TvDAO or 9 mg of Xyl were incubated with 1 g of wet resin in 10 mL of 0.1 M sodium phosphate pH 7 at 25 °C. Upon the immobilization, the samples were incubated with 1M ethanolamine at pH 8 for 2 hours at 25 °C.

Thermal stability studies

Kinetic inactivation through deactivation time-courses at fixed temperature

Thermal stability of immobilized TvDAO was determined by incubating enzyme suspensions in 10 mM phosphate buffer at pH 7 and 50 °C in a thermo-shaker. Similarly, different preparations of immobilized xylanase were incubated at pH 7 and 60 °C. In both cases, suspension samples were taken at different incubation times, and their residual activity was measured as described

above. The experimental data were fitted to from the inactivation time-course were adjusted to a 3-parameters biexponential two-step series inactivation kinetic model³⁸ using the solver tool of Excel Office 365.

Thermodynamic inactivation through thermal-shift assays

3 µg/mL of immobilized enzyme were suspended in 25 mM sodium phosphate buffer and 0.3% of SYPRO® Orange at pH 7 were incubated in a StepOne-plus RT-PCR (Applied Biosystems-ThermoFisher) by using a temperature ramp program from 25-95 °C with a ramp rate of 0.5 °C/min.

Intrinsic protein fluorescence measurements

Fluorescence spectra were carried out with a Varioskan Flash fluorescence spectrophotometer (Thermo Scientific), using an excitation wavelength of 280 nm with excitation and emission bandwidths of 5 nm and recording fluorescence emission spectrum between 300 and 550 nm. All spectroscopic measurements were performed with a solution of 3 µg/mL of immobilized enzyme in 10 mM sodium phosphate at pH 7 and 25 °C.

Oxidation of D-alanine catalyzed by TvDAO immobilized on CEL-G1

100 mg of TvDAO immobilized on CEL-1G were incubated in 400 µL of 10 mM D-Alanine, 0.2 mg/mL Catalase in 50 mM phosphate buffer pH 7 at 25 °C under gently stirring for 4 hours. At different time-points, suspension samples were withdrawn, the immobilized enzymes were separated and the yielded pyruvate in the reaction supernatant was quantified enzymatically using a colorimetric AlaDH assay. Briefly, 10 µL of reaction supernatant were diluted in 190 µL of 0.1 M phosphate buffer pH 7, 0.5 M NH₄Cl and 0.5 mM NADH containing 0.45 U of AlaDH. The

amount of consumed NADH was quantified after 15 minutes at 30 °C. One μmol of consumed NADH is equivalent to one μmol of produced pyruvate. Units of AlaDH (U) are defined as the amount of enzyme needed to convert one μmole of pyruvate into one μmole of L-alanine per minute at the expense of one μmole of NADH, under the reaction conditions described above.

Xylan hydrolysis and XOS synthesis catalyzed by Xyl immobilized on CEL-G1

Xylose and XOS content of samples taken at different times periods during xylan hydrolysis were analyzed by high-performance anion exchange chromatography coupled with pulsed amperometric detection (HPAEC-PAD) using an ICS3000 Dionex system (Dionex Corporation, Sunnyvale, CA) as previously described.²⁶ Identification and quantification of xylose and XOS were based on external calibration using commercial standards and the calibration curve regression coefficients that were higher than 0.99. All samples were previously filtrated through 0.45 μm nylon filters and conveniently diluted with distilled H_2O . All analyses were carried out in triplicate, and data were expressed as the mean value.

Operational stability of the immobilized biocatalysts

The recycling assay of the immobilized biocatalysts was performed under the D-alanine oxidation and Xylan hydrolysis conditions described above for TvDAO and Xyl, respectively. After 2 and 4 hours, the immobilized Xyl and TvDAO, respectively, were recovered by filtering and washing with 10 mM sodium phosphate buffer pH 7. In the following cycle, the immobilized biocatalyst was incubated back with a fresh substrate solution. The retained enzyme activity was

calculated as the ratio between activity at the end of each cycle and activity before the first cycle (expressed as percentage). After each cycle, a sample of the immobilized enzyme was withdrawn, and its intrinsic fluorescence was measured as described above.

ASSOCIATED CONTENT

Supporting Information

The Supporting Information is available free of charge a XXXX.

¹³C CP-MAS-NMR spectrum of 3-glycidoxypropylsilica (Figure S1), ¹³C CP-MAS-NMR spectrum of 3-glycidoxypropylsilica hydrolyzed with HCl (Figure S2), ¹³C CP-MAS-NMR spectrum of 3-glycidoxypropylsilica hydrolyzed with H₂SO₄ (Figure S3), ¹³C CP-MAS-NMR spectrum of 3-glycidoxypropylsilica hydrolyzed with HCl and oxidized with NaIO₄ (Figure S4), ¹³C CP-MAS-NMR spectrum of 3-glycidoxypropylsilica hydrolyzed with H₂SO₄ and oxidized with NaIO₄ (Figure S5), ¹³C CP-MAS-NMR spectrum of glycidoxy-agarose hydrolyzed with H₂SO₄ and oxidized with NaIO₄ (Figure S6), EDX analysis of cellulose-based carriers (Figure S7), normalized intrinsic fluorescence spectrum of TvDAO immobilized on different carriers (Figure S8), thermodynamic denaturation of different heterogeneous biocatalysts of TvDAO using the Thermofluor method (Figure S9), free Xyl stability at pH 10 (Figure S10), fluorescence spectra of Xyl immobilized on different carriers (Figure S11), Xyl loading on AG-G and CEL-G1 (Figure S12), reaction course of xylan degradation (Figure S13), kinetic inactivation of immobilized

enzymes, inactivation constants of TvDAO immobilized on different carriers (Table S1) and inactivation constants of Xyl immobilized on different carriers (Table S2).

AUTHOR INFORMATION

Corresponding Authors

Jose Manuel Guisán - *Department of Biocatalysis, Institute of Catalysis and Petrochemistry (ICP) CSIC, Campus UAM, Cantoblanco, 28049 Madrid, Spain. Email: jmguisan@icp.csic.es*

Fernando López-Gallego - *Heterogeneous Biocatalysis Laboratory, Center for Cooperative Research in Biomaterials (CIC biomaGUNE), Basque Research and Technology Alliance (BRTA), Paseo de Miramón 182, Donostia San Sebastián, Spain. AIKERBASQUE, Basque Foundation for Science, María Díaz de Haro 3, 48013 Bilbao, Spain. Email: flopez@cicbiomagune.es*

Authors

Sandro Martins de Oliveira - *Department of Biocatalysis, Institute of Catalysis and Petrochemistry (ICP) CSIC, Campus UAM, Cantoblanco, 28049 Madrid, Spain*

Susana Velasco-Lozano - *Heterogeneous Biocatalysis Laboratory, Center for Cooperative Research in Biomaterials (CIC biomaGUNE), Basque Research and Technology Alliance (BRTA), Paseo de Miramón 182, Donostia San Sebastián, Spain*

Alejandro H. Orrego - *Department of Biocatalysis, Institute of Catalysis and Petrochemistry (ICP) CSIC, Campus UAM, Cantoblanco, 28049 Madrid, Spain*

Javier Rocha-Martín - *Department of Biocatalysis, Institute of Catalysis and Petrochemistry (ICP) CSIC, Campus UAM, Cantoblanco, 28049 Madrid, Spain. orcid.org/0000-0002-7681-5439*

Sonia Moreno-Pérez - *Department of Biocatalysis, Institute of Catalysis and Petrochemistry (ICP) CSIC, Campus UAM, Cantoblanco, 28049 Madrid, Spain*

José M. Fraile - *Instituto de Síntesis Química y Catálisis Homogénea (ISQCH), CSIC-University of Zaragoza, Pedro Cerbuna, 12, Zaragoza, Spain*

Author Contributions

The manuscript was written through the contribution of all authors. All authors have given approval to the final version of the manuscript.

Funding

The authors acknowledge funding from the National Council for Scientific and Technological Development (CNPq) for financial support for the PhD scholarships of S.M.O (Process CsF 201683/2014-2008). J.M.G thanks the funding from the EU FP7 project Lignofood (Ingredients for Food and Beverage Industry from a Lignocellulosic Source, grant agreement nº 606073). F.L-G acknowledges the funding of IKERBASQUE. This work was performed under the Maria de Maeztu Units of Excellence Program from the Spanish State Research Agency – Grant No. MDM-2017-0720. J.M.F. thanks the funding from the Spanish Ministerio de Ciencia e Innovación (grant RTI2018-093431-BI00).

Author Contributions

The manuscript was written through contributions of all authors. All authors have given approval to the final version of the manuscript. ‡These authors contributed equally.

ABBREVIATIONS USED

TvDAO, D-amino acid oxidase from *Trigonopsis variabilis*; Xyl, xylanases from *Trichoderma reesei*; XOS, xylooligosaccharides; EPI, epichlorhydrin (EPI); CEL-G, oxidized cellulose macroporous beads without activation/hydrolysis; CEL-G1, cellulose macroporous beads activated with rac-glycidol and further oxidized with NaIO₄; CEL-SG2, cellulose macroporous beads activated with epichlorhydrin, hydrolyzed with H₂SO₄ and further oxidized with NaIO₄; CEL-HG2, cellulose macroporous beads activated with epichlorhydrin, hydrolyzed with HCl and further oxidized with NaIO₄; AG-G, agarose macroporous beads activated with glyoxyl groups; AG-CB: agaros macroporous beads activated with cyanogen bromide groups. ¹³C CP-MAS-NMR, Cross-Polarization Magic Angle Spinning Carbon-13 Nuclear Magnetic Resonance.

REFERENCES

1. DiCosimo, R.; McAuliffe, J.; Poulou, A. J.; Bohlmann, G., Industrial use of immobilized enzymes. *Chem. Soc. Rev.* **2013**, 42, (15), 6437-6474.
2. Basso, A.; Serban, S., Industrial applications of immobilized enzymes—A review. *Molecular Catalysis* **2019**, 479, 110607.
3. Garcia-Galan, C.; Berenguer-Murcia, Á.; Fernandez-Lafuente, R.; Rodrigues, R. C., Potential of Different Enzyme Immobilization Strategies to Improve Enzyme Performance. *Adv. Synth. Catal.* **2011**, 353, (16), 2885-2904.
4. Guisan, J. M.; López-Gallego, F.; Bolivar, J. M.; Rocha-Martín, J.; Fernandez-Lorente, G., The science of enzyme immobilization. In *Immobilization of Enzymes and Cells: Methods and Protocols*, Guisan, J. M.; Bolivar, J. M.; López-Gallego, F.; Rocha-Martín, J., Eds. Springer US: New York, NY, 2020; pp 1-26.
5. Cantone, S.; Ferrario, V.; Corici, L.; Ebert, C.; Fattor, D.; Spizzo, P.; Gardossi, L., Efficient immobilisation of industrial biocatalysts: criteria and constraints for the selection of organic polymeric carriers and immobilisation methods. *Chem. Soc. Rev.* **2013**, 42, (15), 6262-6276.

6. Zucca, P.; Fernandez-Lafuente, R.; Sanjust, E., Agarose and its derivatives as supports for enzyme immobilization. *Molecules* **2016**, *21*, (11), 1577.
7. Cuatrecasas, P., Protein purification by affinity chromatography: Derivatizations of agarose and polyacrylamide beads. *J. Biol. Chem.* **1970**, *245*, (12), 3059-3065.
8. Pellis, A.; Cantone, S.; Ebert, C.; Gardossi, L., Evolving biocatalysis to meet bioeconomy challenges and opportunities. *New Biotechnology* **2018**, *40*, 154-169.
9. Klemm, D.; Heublein, B.; Fink, H.-P.; Bohn, A., Cellulose: Fascinating biopolymer and sustainable raw material. *Angew. Chem. Int. Ed.* **2005**, *44*, (22), 3358-3393.
10. Östlund, Å.; Idström, A.; Olsson, C.; Larsson, P. T.; Nordstierna, L., Modification of crystallinity and pore size distribution in coagulated cellulose films. *Cellulose* **2013**, *20*, (4), 1657-1667.
11. Gericke, M.; Trygg, J.; Fardim, P., Functional cellulose beads: Preparation, characterization, and applications. *Chem. Rev.* **2013**, *113*, (7), 4812-4836.
12. Sandig, B.; Michalek, L.; Vlahovic, S.; Antonovici, M.; Hauer, B.; Buchmeiser, M. R., A monolithic hybrid cellulose-2.5-acetate/polymer bioreactor for biocatalysis under continuous liquid-liquid conditions using a supported ionic liquid phase. *Chem. Eur. J.* **2015**, *21*, (44), 15835-15842.
13. Mateo, C.; Palomo, J. M.; Fuentes, M.; Betancor, L.; Grazu, V.; López-Gallego, F.; Pessela, B. C. C.; Hidalgo, A.; Fernández-Lorente, G.; Fernández-Lafuente, R.; Guisán, J. M., Glyoxyl agarose: A fully inert and hydrophilic support for immobilization and high stabilization of proteins. *Enzyme and Microbial Technology* **2006**, *39*, (2), 274-280.
14. Fernandez-Lorente, G.; Lopez-Gallego, F.; M. Bolivar, J.; Rocha-Martin, J.; Moreno-Perez, S.; M. Guisan, J., Immobilization of Proteins on Highly Activated Glyoxyl Supports: Dramatic Increase of the Enzyme Stability via Multipoint Immobilization on Pre-existing Carriers. *Curr. Org. Chem.* **2015**, *19*, (17), 1719-1731.
15. Sonawane, V. C., Enzymatic Modifications of Cephalosporins by Cephalosporin Acylase and Other Enzymes. *Critical Reviews in Biotechnology* **2006**, *26*, (2), 95-120.
16. Polizeli, M. L. T. M.; Rizzatti, A. C. S.; Monti, R.; Terenzi, H. F.; Jorge, J. A.; Amorim, D. S., Xylanases from fungi: properties and industrial applications. *Applied Microbiology and Biotechnology* **2005**, *67*, (5), 577-591.
17. Santibáñez, L.; Henríquez, C.; Corro-Tejeda, R.; Bernal, S.; Armijo, B.; Salazar, O., Xylooligosaccharides from lignocellulosic biomass: A comprehensive review. *Carbohydrate Polymers* **2021**, *251*, 117118.
18. Lindh, J.; Carlsson, D. O.; Strømme, M.; Mihranyan, A., Convenient one-pot formation of 2,3-dialdehyde cellulose beads via periodate oxidation of cellulose in water. *Biomacromolecules* **2014**, *15*, (5), 1928-1932.
19. Potthast, A.; Kostic, M.; Schiehser, S.; Kosma, P.; Rosenau, T., Studies on oxidative modifications of cellulose in the periodate system: Molecular weight distribution and carbonyl group profiles. *Holzforschung* **2007**, *61*, (6), 662.
20. Fauré, N. E.; Halling, P. J.; Wimperis, S., A solid-state NMR study of the immobilization of α -chymotrypsin on mesoporous silica. *J. Phys. Chem. C* **2014**, *118*, (2), 1042-1048.
21. Xu, Z.-Q.; Qiu, Y.-L.; Chokekijchai, S.; Mitsuya, H.; Zemlicka, J., Unsaturated acyclic analogs of 2'-deoxyadenosine and thymidine containing fluorine: Synthesis and biological activity. *J. Med. Chem.* **1995**, *38*, (6), 875-882.

22. Nigro, M. J.; Brardinelli, J. I.; Lewkowicz, E. S.; Iribarren, A. M.; Laurella, S. L., Aldehyde-hydrate equilibrium in nucleobase 2-oxoethyl derivatives: An NMR, ESI-MS and theoretical study. *J. Mol. Struct.* **2017**, 1144, 49-57.
23. Kahyaoglu, A.; Haghjoo, K.; Kraicsovits, F.; Jordan, F.; Polgar, L., Benzyloxycarbonylprolylprolinal, a transition-state analogue for prolyl oligopeptidase, forms a tetrahedral adduct with catalytic serine, not a reactive cysteine. *Biochemical Journal* **1997**, 322, (3), 839-843.
24. Kuwae, A.; Hanai, K.; Oyama, K.; Uchino, M.; Lee, H.-H., Solid state structures of phenylpyruvates as studied by high resolution ¹³C NMR spectroscopy. *Spectrochim. Acta, Pt. A: Mol. Spectrosc.* **1993**, 49, (1), 125-133.
25. Lee, C. M.; Mittal, A.; Barnette, A. L.; Kafle, K.; Park, Y. B.; Shin, H.; Johnson, D. K.; Park, S.; Kim, S. H., Cellulose polymorphism study with sum-frequency-generation (SFG) vibration spectroscopy: identification of exocyclic CH₂OH conformation and chain orientation. *Cellulose* **2013**, 20, (3), 991-1000.
26. Martins de Oliveira, S.; Moreno-Perez, S.; Romero-Fernández, M.; Fernandez-Lorente, G.; Rocha-Martin, J.; Guisan, J. M., Immobilization and stabilization of commercial β-1,4-endoxylanase Depol™ 333MDP by multipoint covalent attachment for xylan hydrolysis: Production of prebiotics (xylo-oligosaccharides). *Biocatal. Biotransform.* **2018**, 36, (2), 141-150.
27. He, J.; Tang, F.; Chen, D.; Yu, B.; Luo, Y.; Zheng, P.; Mao, X.; Yu, J.; Yu, F., Design, expression and functional characterization of a thermostable xylanase from *Trichoderma reesei*. *PLoS One* **2019**, 14, (1), e0210548.
28. Kar, S.; Sona Gauri, S.; Das, A.; Jana, A.; Maity, C.; Mandal, A.; Das Mohapatra, P. K.; Pati, B. R.; Mondal, K. C., Process optimization of xylanase production using cheap solid substrate by *Trichoderma reesei* SAF3 and study on the alteration of behavioral properties of enzyme obtained from SSF and SmF. *Bioprocess and Biosystems Engineering* **2013**, 36, (1), 57-68.
29. Henley, J. P.; Sadana, A., Deactivation theory. *Biotechnol. Bioeng.* **1986**, 28, (8), 1277-1285.
30. Bommarius, A. S.; Paye, M. F., Stabilizing biocatalysts. *Chemical Society Reviews* **2013**, 42, (15), 6534-6565.
31. Romero-Fernández, M.; Moreno-Perez, S.; Martins de Oliveira, S.; Santamaría, R. I.; Guisan, J. M.; Rocha-Martin, J., Preparation of a robust immobilized biocatalyst of β-1,4-endoxylanase by surface coating with polymers for production of xylooligosaccharides from different xylan sources. *N. Biotechnol.* **2018**, 44, 50-58.
32. de Oliveira, S. M.; Moreno-Perez, S.; Terrasan, C. R. F.; Romero-Fernández, M.; Vieira, M. F.; Guisan, J. M.; Rocha-Martin, J., Covalent immobilization-stabilization of β-1,4-endoxylanases from *Trichoderma reesei*: Production of xylooligosaccharides. *Process Biochem.* **2018**, 64, 170-176.
33. da Silva, E. S.; Gomez-Vallejo, V.; Baz, Z.; Llop, J.; Lopez-Gallego, F., Efficient Enzymatic Preparation of N-13-Labelled Amino Acids: Towards Multipurpose Synthetic Systems. *Chemistry-a European Journal* **2016**, 22, (38), 13619-13626.
34. McCluer, R. H., Methods in carbohydrate chemistry. Volume 1, analysis and preparation of sugars (Whistler, Roy L.; Wolfrom, M. L.; ed.s). *J. Chem. Educ.* **1963**, 40, (5), A394.
35. Guisán, J., Aldehyde-agarose gels as activated supports for immobilization-stabilization of enzymes. *Enzyme and Microbial Technology* **1988**, 10, (6), 375-382.

36. Fornera, S.; Walde, P., Spectrophotometric quantification of horseradish peroxidase with *o*-phenylenediamine. *Anal. Biochem.* **2010**, 407, (2), 293-295.
37. Miller, G. L., Use of dinitrosalicylic acid reagent for determination of reducing sugar. *Anal. Chem.* **1959**, 31, (3), 426-428.
38. Aymard, C.; Belarbi, A., Kinetics of thermal deactivation of enzymes: a simple three parameters phenomenological model can describe the decay of enzyme activity, irrespectively of the mechanism. *Enzyme Microb. Technol.* **2000**, 27, (8), 612-618.